Surveys in Geophysics (2021) 42:1425–1442
https://doi.org/10.1007/s10712-021-09665-1

A New Instrumental Array in Sichuan, China, to Monitor Vibrations and Perturbations of the Lithosphere, Atmosphere, and Ionosphere

Chieh-Hung Chen[1,2] · Yang-Yi Sun[1] · Kai Lin[1] · Chen Zhou[3] · Rui Xu[4] · Haiyin Qing[5] · Yongxin Gao[6] · Tao Chen[7] · Fei Wang[8] · Huaizhong Yu[9] · Peng Han[10] · Chi-Chia Tang[1] · Xiaoning Su[11] · Xuemin Zhang[12] · Linguo Yuan[13] · Yixian Xu[14] · Jann-Yenq Liu[15,16,17] · Shunkuan Yu[18]

Received: 2 July 2021 / Accepted: 17 September 2021 / Published online: 19 October 2021

Abstract
Scientists investigating the coupling between the lithosphere, atmosphere, and ionosphere (LAI) require multiple instruments installed on and near the Earth's surface and aboard satellites orbiting the Earth. However, challenges always occur owing to a lack of observation data from other monitoring instruments and/or the distance between distinct instruments. A novel system for monitoring vibrations and perturbations in the LAI (MVP–LAI) was established in the countryside of Leshan City, Sichuan Province, China, in June 2021. Twelve different types of instruments with 18 devices were set within an area of 50 m × 50 m. The other two were installed approximately 20 km away to avoid interference. These instruments routinely monitor the changes in at least 14 geophysical parameters with short sampling intervals, available for capturing waves propagating from the subsurface to the ionosphere. Once the observations retrieved from the China Seismo-Electromagnetic Satellite and the radio occultation are integrated, the monitoring of vibrations and perturbations can reach ~ 800 km above the Earth's surface. The system is mainly operated by the China University of Geoscience (Wuhan), China and will officially start functioning in September 2021. All the efforts benefit the investigation of the causal mechanisms of LAI coupling and expose the potential sources of vibrations and perturbations, incorporating observations from other spheres.

Keywords Lithosphere–Atmosphere–Ionosphere coupling · MVP-LAI system · Vertical vibrations and perturbations · Atmospheric-gravity wave

✉ Chieh-Hung Chen
nononochchen@gmail.com

Extended author information available on the last page of the article

Article Highlights

- A novel system has been established in Southwest China to study the Lithosphere–Atmosphere–Ionosphere (LAI) coupling
- 12 different instruments were mainly installed within an area of ~ 2500 m^2 for monitoring vertical perturbations in LAI
- The instrumental array is utilized to capture perturbations between − 5 m underground and ~350 km in altitude

1 Introduction

Coupling of Earth's spheres from the subsurface to space has drawn the interest of scientists for decades. Numerous studies (Huang et al. 1985; Gokhberg et al. 1989; Davies 1990; Gufeld et al. 1992; Hayakawa et al. 1996a; Molchanov and Hayakawa 1998; Bishop and Straus 2006; Liu et al. 2006a,b, 2016a,b; Rishbeth 2006; Hayakawa 2007, 2011; Xiao et al. 2007; Oyama et al. 2008; Xu et al. 2008; Chakrabarti 2010; Hayakawa and Hobara 2010; Sun et al. 2011; Polyakova and Perevalova 2011; Rozhnoi et al. 2013; Ryu et al. 2015; Sorokin et al. 2015; Kelley et al. 2017; Zhou et al. 2017; Astafyeva 2019; Laštovička and Šindelářová 2019) reported that activities in the lithosphere, atmosphere, and ionosphere (LAI) are interactive.

Changes in the lower atmosphere can drive ionospheric dynamics and structures. The planetary-scale distribution of convection in the troposphere along the equator (e.g., Walker circulation) can induce the wave-four structure of the equatorial ionospheric anomaly (Immel et al. 2006; Lin et al. 2007; Wan et al. 2008). Atmospheric tides and planetary waves comprise the largest portion of the well-known wave-four structure (Chang et al. 2013, 2016). The El Niño—Southern Oscillation (ENSO) is the most significant dynamic driver of inter-annual variations in the troposphere. ENSO significantly changes the circulation and distribution of convections that modulate the quasi-biennial oscillation of wind and tides from the stratosphere to the ionosphere (Sun et al. 2018, 2019).

Severe weather activities in the troposphere generate atmospheric gravity waves (AGWs) that propagate upward to the ionosphere and induce traveling ionospheric disturbances and irregularities. For example, Xiao et al. (2007) examined the data of the ionospheric HF Doppler shift during 24 strong typhoons from 1987 to 1992. Their analysis revealed the common features of ionospheric responses to typhoons. They suggested that typhoons are an effective wave source especially when a typhoon is landing on or near a mainland coast. Nishioka et al. (2013) examined the ground-based Global Navigation Satellite System (GNSS) total electron content (TEC) observations and showed concentric waves in the ionosphere after an enhanced Fujita scale (EF-scale) 5 tornado in Moore, Oklahoma, on 20 May 2013. Chou et al. (2017a, 2017b) examined the TEC data and reported that the super typhoons Meranti and Nepartak in 2016 induced concentric traveling ionospheric disturbances and plasma instabilities. Moreover, solar eclipses can trigger AGWs in the lower atmosphere that propagate upward and induce bow waves and irregularities in the ionosphere (Liu et al. 2011a; Wang et al. 2021). Sun et al. (2021a) reported TEC perturbations with wavelength of ~ 2700 km and period of ~ 3.5 h due to the annular solar eclipse in the nighttime on 21 June 2020. The large-scale perturbations propagating in a northwestward direction after sunset behave as a solar terminator wave. However, the exact origin of the eclipse-induced atmospheric gravity waves have not yet been identified

due to the complex of the ionosphere influenced from the lower-lying atmospheric regions (Koucká Knížová et al. 2021).

Large surface waves due to tsunami or earthquakes can trigger significant ionospheric disturbances (Liu et al. 2006a,b, 2011b; Kakinami et al. 2012; Chum et al. 2016). The large ocean waves of tsunami reflected by multiple sources, such as seamounts, islands, and ridges, can excite tremendous ionospheric and atmospheric waves that propagate in various directions, cross at arbitrary angles (Sun et al. 2021b), and keep the ionosphere disturbed for hours to days (Chou et al. 2020; Yan et al. 2018). On the other hand, space weathers due to solar activities, such as coronal mass ejection, solar wind blowing, flare, and eclipse, can largely disturb the Earth's magnetic field, electric field, plasma distribution, and current systems, as well as the thermospheric neutral density, compositions, temperature, and winds that further modulate the ionospheric dynamics (Cander 2019; Materassi et al. 2020; Liu and Wan 2020). The mixture of both the impacts from above (from solar) and below (near surface) causes investigating the origin, propagation, and evolution of waves and perturbations in different Earth's spheres remaining challenging (Sun 2019). Numerous studies have made great efforts to unravel the complex ionospheric disturbances caused by changes in climate and weather in the lower troposphere and surface waves; however, this issue is still under investigation because the disturbances are much more persistent and complicated than previously thought.

The LAI coupling can be excited by sources in the lithosphere through promising channels (Hayakawa 2015, 2016). Gas release near the Earth's surface perturbs the conductivity in the atmosphere and changes the atmospheric electric field, leading to ionospheric modification (Pulinets and Boyarchuk 2004; Sorokin et al. 2006; Pulinets and Ouzounov 2011; Harrison et al. 2010, 2014). An increase in subsurface conductivity can excite the occurrence of cloud-to-ionosphere lighting that changes in the ionosphere through heating and/or ionization processes (Inan et al. 1991; Pasko et al. 1997; Cho and Rycroft 1998; Rodger 1999; Takahashi et al. 2003; Hayakawa et al. 2004). Acoustic gravity waves close to the Earth's surface can be generated by variations in temperature and/or ground vibrations (VanZandt 1985; Davies 1990; Tsuda et al. 1994; De la Torre et al., 1999; Hickey et al. 2001; Sun et al. 2016; Chou et al. 2020; Yang et al. 2019, 2020; Yang and Hayakawa 2020; Chen et al., 2020, 2021a). The upward propagation of acoustic gravity waves can perturb the electron density in the ionosphere (Molchanov et al. 2001; Miyaki et al. 2002; Shvets et al. 2004; Korepanov et al. 2009; Kasahara et al. 2010; Hayakawa 2011; Sun et al. 2011, 2016; Oyama et al. 2016; Liu et al. 2016c; Chum et al. 2016). On the other hand, variations in the electromagnetic field can directly induce changes in the ionosphere due to radio emissions (Fraser-Smith et al. 1990; Molchanov et al. 1993, 1995; Molchanov and Hayakawa 1995; Hayakawa et al. 1996b).

In contrast, responses in the lithosphere can be caused by perturbations from space and the ionosphere. The energy carried by solar winds can influence the electromagnetic field around the Earth's surface through electromagnetic coupling (Pulinets 2009). The energy can change the ionospheric current at an altitude of ~ 100 km, dominating the diurnal variations of the geomagnetic field near the Earth's surface (Yamazaki and Maute, 2016). On the other hand, the electromagnetic field near the Earth's surface can be changed by geomagnetically induced currents because electrically charged particles pass through the ionosphere (Lucas et al. 2020). These aforementioned studies propose promising mechanisms for perturbations and vibrations in one sphere, causing changes in the other two. However, a system comprising numerous instruments that can monitor the process of perturbations and/or vibrations between the ground and space at particular altitudes is insufficient.

In 2021, a novel system was established in Sichuan, China (29.6°N, 103.9°E) to monitor vibrations and perturbations in the LAI (the MVP-LAI system). The system is located on the western side of the Sichuan Basin and the eastern margin of the Tibet Plateau. A noticeable discrepancy of approximately 3000 m in altitude between the Sichuan Basin and the Tibet Plateau provides an excellent opportunity for monitoring vibrations and perturbations in the vertical direction. The system comprises 14 different instruments with a total of 22 devices that monitor changes in at last 14 distinct geophysical parameters for capturing vibrations and perturbations in the vertical direction, from the lithosphere to the ionosphere. These efforts are beneficial for understanding the physical processes of perturbations and investigating the promising sources in LAI coupling.

2 The New Equipment for Monitoring Vibrations and Perturbations in the Lithosphere, Atmosphere and Ionosphere

The core location of the MVP-LAI system occupies ~ 400 m^2 (20 m × 20 m). Twelve distinct instruments were installed on and around the core place (Fig. 1). A piezometer was placed at the bottom of the well at a depth of 5 m to monitor changes in water levels with a sampling interval of 2 s (please find more detailed information on the instruments in Table 1). Changes in air temperature in the wells 1, 3, and 5 m in depth and at 1.5 m above the Earth's surface were recorded by four thermometers with a sampling interval of 1 min. Barometers were tied together with thermometers to monitor variations in air pressure at particular depths and altitudes. Two broadband seismometers with a sampling interval of

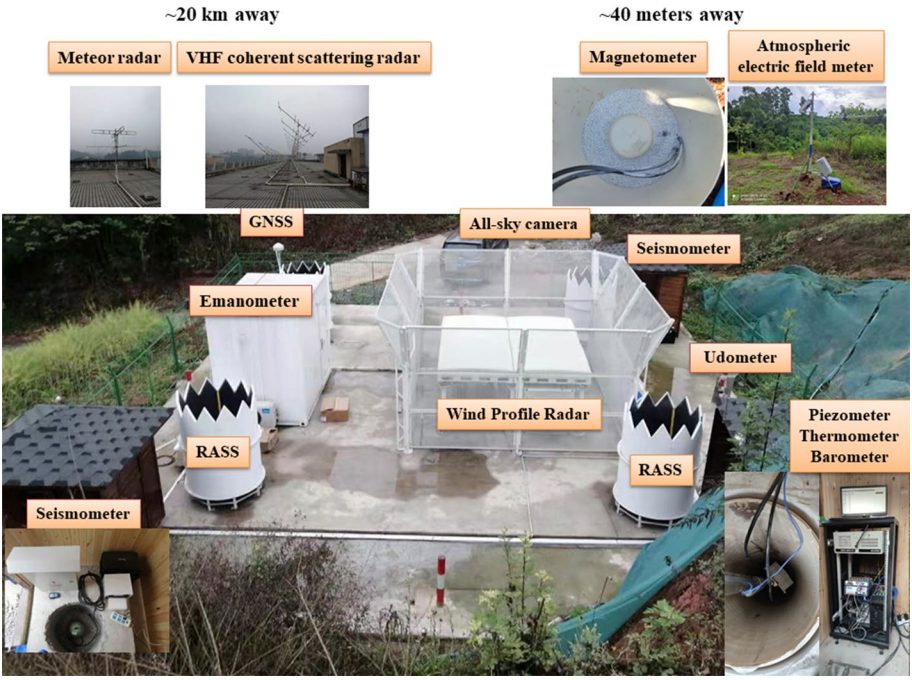

Fig. 1 Photograph of the MVP-LAI system

Table 1 Information of the instruments utilized in the MVP-LAI system

Instrument	Model	Manufacturing nation	Resolution	Sampling interval	Observation parameter	Note
VHF coherent scattering radar	WHU VHF	Australia	Altitude:2 km	300 s = 5 min	Ionospheric irregularity	
Meteor radar	WHU MET	Australia	Altitude: 2 km	3600 s = 1 h	Air density, and temperature	
Wind Profile Radar (WPR) Radio Acoustic Sounding System (RASS)	CLC-11-D	China	Wind velocity: 0.2 m/s Wind azimuth: 0.5° Temperature: 1 °C Altitude: 60 m for the low mode 120 m for the high mode	60 s	Wind azimuth and velocity Temperature	From 8:00 LT to 20:00 LT, first 55 min for WPR and last 5 min for RASS, from 20:00 LT to 8:00 LT for WPR only
All sky camera	ASI2900MM	China	1939 × 1096 pixels	3600 s = 1 h	Cloud shape	
Udometer	WS100	USA	0.01 mm	3600 s = 1 h	Precipitation	
GNSS	GR50	Switzerland		1 s	Crustal deformation, and TEC	
Atmospheric electric conductivity meter	DDL8364-01	China	10^{-15} S/m	30 min	Air conductivity	After December in 2021
Atmospheric electric field meter	DNDY-2	China	0.1 V/m	1 s	Surface electric field	
	CS110	USA	0.32 V/m for 0–2200 V/m 3.2 V/m for 2200–22,300 V/m	1 s		
Emanometer	AlphaGUARD P2000F	Germany	Air pressure: 0.1 hPa Temperature: 0.2 °C Relative air humidity: 0.2% rH Radon concentration: 0.01 pCi/l	600 s = 10 min	Radon concentration	
Broadband seismometer	Trillium 120 QA	Canada		0.01 s	Ground vibrations	Two devices at the MVP-LAI station

Table 1 (continued)

Instrument	Model	Manufacturing nation	Resolution	Sampling interval	Observation parameter	Note
Magnetometer	HS-MS-DM3R and T-50	China	0.1 nT	0.02 s	Magnetic field, ionosphere current, and underground conductivity	Before September in 2021
	FRG-604RC	Japan	0.01 nT	0.1 s		After October in 2021
Barometer	PTB330	Finland	0.01 hPa	2 s	Air pressure	In the holes with depths of 5, 3 and 1 m and 1.5 m above the surface
Piezometer	MIK-P260	China	0.001 m	2 s	Ground water level	In the hole of -5 m
Thermometer	MILLIK	UK	0.0001 °C	60 s	Temperature	In the holes with depths of 5, 3 and1 m and 1.5 m above the surface

0.01 s were installed at the opposite side of the core place for investigating an azimuth of ground vibrations propagating around the MVP-LAI system. A ground-based GNSS receiver was installed on the core place to receive electromagnetic signals with a sampling interval of 1 s. The signals emitted from GNSS satellites are utilized to monitor crustal deformation. Meanwhile, the signals from the geostationary satellites of the BeiDou navigation system (BDS) (Su et al. 2018) reveals changes in the TEC ~ 350 km in altitude over certain locations 24–7 without interruption. An all sky camera with 1939 × 1096 pixels was placed on the roof of a log cabin to observe variations in clouds. WPR (wind profile radar), and RASS (radio acoustic sounding system) were set at the center of the place. The WPR and RASS were utilized to observe changes in temperatures, velocities, and azimuths of winds along the vertical direction from the subsurface to ~ 4 km in altitude. An udometer monitor precipitation around the system for corrections of water level records and clarify the impacts on the vertical electric field near the Earth's surface due to rainfall. An emanometer was utilized to monitor changes in radon concentration in the air to investigate the relationship between the composition of air and the electric field near the Earth's surface. A magnetometer and two atmospheric electric field meters were located approximately 40 m away from the core place. The magnetometer is used to observe variations in conductivity underground (Parkinson and Jones 1979; Chen et al. 2013, 2015; Mao et al. 2020), changes in the geomagnetic field near the Earth's surface (Gao et al. 2016, 2020; Chen et al. 2017, 2021b), lightning in the troposphere (Fraser-Smith and Kjono 2014), and changes in electric currents at ~ 100 km in altitude above the MVP-LAI system (Yamazaki and Maute, 2016). Records from atmospheric electric field meters can be utilized to study fluctuations in the vertical electric field near the Earth's surface, which is beneficial for exposing lightning in the atmosphere. A meteor radar and a very high frequency (VHF) coherent scattering radar operated by the Wuhan University were located ~ 20 km southwest away from the core to detect temperature and density in the atmosphere at ~ 80 km above the Earth's surface and plasma irregularities at approximately 90–160 km in altitude, respectively. These instruments are integrated to monitor variations of more than 14 geophysical parameters, mainly ranging between -5 m underground and ~ 350 km in altitude, simultaneously and to further examine the proposed promising mechanisms (Hayakawa 2015, 2016) of LAI coupling. Additionally, once observation data retrieved from the China Seismo-Electromagnetic Satellite (Shen et al. 2018a, 2018b) and radio occultation (Sun et al. 2016; Rajesh et al. 2021) are integrated, vibrations and perturbations existing between the subsurface and an altitude of ~ 800 km in altitude were captured.

3 Study Plans and Preliminary Results

The MVP-LAI system can be utilized to examine the promising mechanisms reported in previous studies (Hayakawa 2015, 2016). Once TEC variations in the ionosphere are caused by radon release, the emanometer can detect changes in radon concentration near the Earth's surface. Anomalous phenomena in the atmospheric electric field can be monitored using an atmospheric electric field meter. In addition, no noticeable anomaly was found in the other geophysical parameters. On the other hand, variations in TEC in the ionosphere can result from an increase in conductivity underground. Changes in underground conductivity can be investigated by using the magnetic data through the Parkinson vector (Parkinson 1962; Parkinson and Jones 1979) and understood by the increase and depression of groundwater levels monitored by the piezometer. If acoustic gravity waves

are excited by changes in temperature and/or ground vibrations, the associated variations can be detected by thermometers and broadband seismometers through the frequency analysis method. Once acoustic gravity waves propagate upward, driving changes in the atmosphere, velocities, and azimuths of winds and the temperature profiles from the surface to a few kilometers above change accordingly, which can be detected by using WPR and RASS. In addition, variations in the TEC can be caused by electromagnetic emission. The sources of electromagnetic emissions can be detected using data from magnetometers and broadband seismometers. Once TEC variations are not dominated by the aforementioned promising mechanisms, the examination of numerous geophysical parameters monitored using the MVP-LAI system are beneficial for exposing the potential sources and causal mechanisms. When perturbations in the ionosphere trigger ground vibrations due to changes in air pressure, responses to geophysical parameters in the atmosphere and the lithosphere can be detected by the magnetometer, barometers, and broadband seismometers. If the perturbations trigger responses in the lithosphere due to electromagnetic induction, anomalous phenomena can be observed in the electric and magnetic fields but not in the air pressure and ground vibration. In short, aforementioned potential mechanisms of the LAI coupling can be directly examined by comparison among multiple observation data retrieved from different instruments through cross correlation methods in the temporal domain. Once observation data reveal potential relationships, they are transferred into the frequency domain by using the Fourier transform and/or the wavelet transform to investigate frequency characteristics of different physical parameters. Pronounced frequencies are compared with the results in previous studies for further determine causal mechanisms. Novel mechanisms would be found through repeated examination and inductive reasoning.

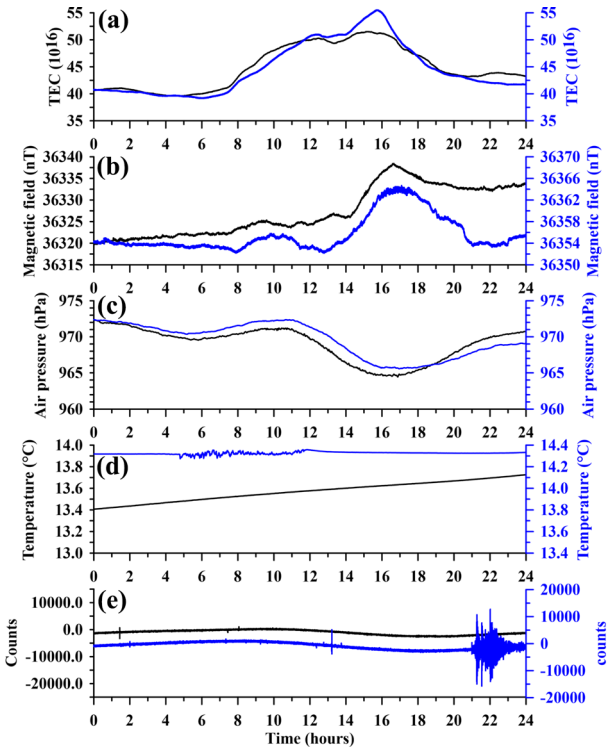

Fig. 2 Variations of the temperature, seismic, air pressure, magnetic, and TEC data recorded on 6 and 10 February 2021. The black and blue curves denote the variations of the recorded data on 6 and 10 February 2021, respectively; **a**–**e** show the TEC, magnetic, air pressure data, temperature, and ground vibrations, respectively

Before the official function of the MVP-LAI system, some interesting phenomena were observed using partial instruments. Figure 2 shows the variations in temperature, ground vibrations, air pressure, geomagnetic field, and GNSS-TEC on 6 and 10 February 2021. Unusual TEC variations, namely two relatively local maxima, were found at ~ 12:00 LT, and ~ 16:00 LT on 6 February 2021 (Fig. 2a). This is significantly different from the signal maximum appearing at ~ 14:00 LT under normal conditions. No significant relationship was directly obtained from the comparison between the unusual TEC variations and other data (i.e., the geomagnetic field, air pressure, and temperature) in Fig. 2. We transferred these data into the frequency domain using the Fourier transform as shown in Fig. 3. Variations of TEC in a frequency band between 0.0009 Hz and 0.003 Hz on 10 February 2021 are shown in Fig. 3a. Enhancements of amplitude in the frequency < 0.001 Hz are mainly ranged between ~ 8:00 LT and ~ 20:00 LT due to solar radiation. In contrast, enhancements of the amplitude in the frequency band of 0.001–0.002 Hz begin at ~ 8:00 LT, ~ 12:00 LT and ~ 16:00 LT. Enhancements can also be found at a frequency of ~ 0.0035 Hz for the magnetic field (Fig. 3b), at a frequency of ~ 0.002 Hz for the air pressure (Fig. 3c) and at a frequency of ~ 0.002 Hz for the temperature (Fig. 3d) at ~ 08:00 LT and ~ 17:00 LT. Figure 3e shows that the frequency characteristics of gravity waves vary from the subsurface to 350 km in altitude (Hines 1960; Chou et al. 2017a). An agreement between gravity waves and the enhancements at distinct geophysical parameters (Fig. 3a–d) in the frequency characteristics at distinct altitudes suggests that the local maxima of the TEC variations at ~ 08:00 LT and ~ 17:00 LT can be attributed to variations in the air pressure and temperature near the ground. In contrast, no significant enhancement can be observed in the

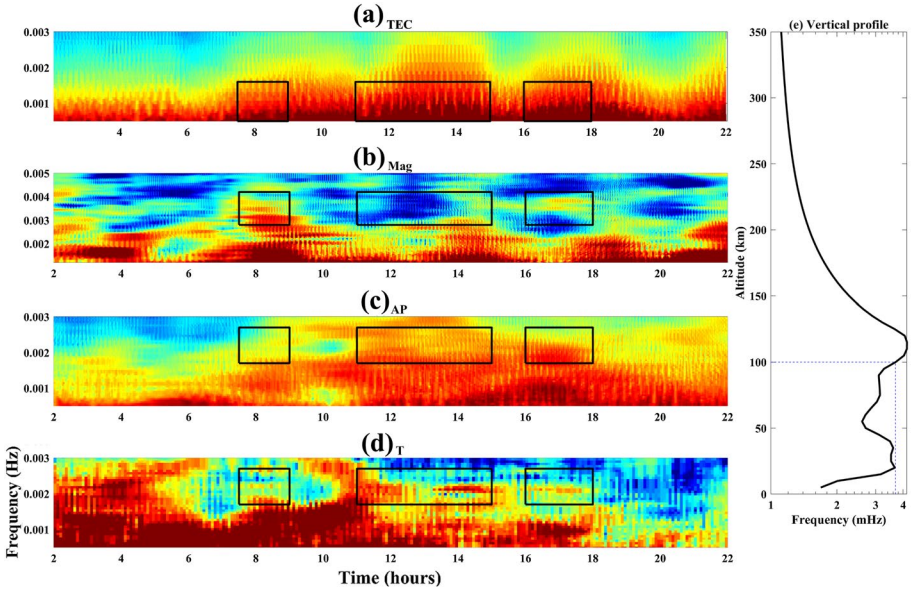

Fig. 3 Amplitude of the TEC, magnetic, air pressure, and temperature data on 10 February 2021 and the frequency characteristics of gravity waves varying from the Earth's surface to 350 km in altitude; **a**–**d** show the amplitude of the TEC, magnetic (Mag), air pressure (AP), and temperature (T) data using the short-term Fourier transform on 10 February 2021. Frequency characteristics of gravity waves vary from the Earth's surface to the 350 km in altitude are computed using the model and parameters in Hines (1960) and Chou et al. (2017a) shown in (**e**)

geomagnetic data at ~ 16:00 LT. This suggests that the enhancements of TEC at ~ 16:00 LT are irrelevant to the contribution of gravity waves.

On 10 February 2021 earthquakes with magnitudes of 6.3, 6.1, and 7.7 occurred in Indonesia at 19:52:27 (UTC + 8) and southeast of the Loyalty Islands at 20:01:59 and 21:19:55 (UTC + 8), respectively (see the associated information at USGS). Surface waves for these earthquakes arrived at the MVP-LAI system at ~ 20:32:40 LT, ~ 20:43:6 LT, and ~ 21:55:26 LT, as shown in Fig. 2d. However, no significant perturbation and/or disturbance triggered by the arrival of the surface waves can be directly found from the raw data shown in Fig. 2a–c. Variations in the TEC triggered by the upward propagation of acoustic waves due to the arrival of the surface waves (i.e., Rayleigh waves) in the frequency and temporal domains are shown in Figs. 4a–d and 5a–d, respectively. The air pressure changes accordingly in a similar frequency band (i.e., 0.01–0.03 Hz) as per the arrivals of the surface waves (Fig. 4c–d). Variations in the geomagnetic field and TEC occur ~ 11 min after the arrival of surface waves because the upward propagation of acoustic waves from the lithosphere to the ionosphere takes ~ 11 min (Fig. 4a–b). The ground vibrations, magnetic field and TEC roughly share frequencies at 0.01–0.03 Hz. We further filtered these data using a band-pass filter with related frequency bands and focused on the data segments of the arrival of the Rayleigh waves triggered by the M7.7 earthquake (Fig. 5). Amplitude of the filtered data decrease after the wave arrivals that can be found in ground vibrations and air pressure (Fig. 5d). Variations in the filtered magnetic and TEC data are shifted by ~ 11 min for an effective comparison with the arrivals of the Rayleigh waves (Fig. 5c–d). Variations in the envelopes for the seismic, magnetic, and TEC data yield an approximate

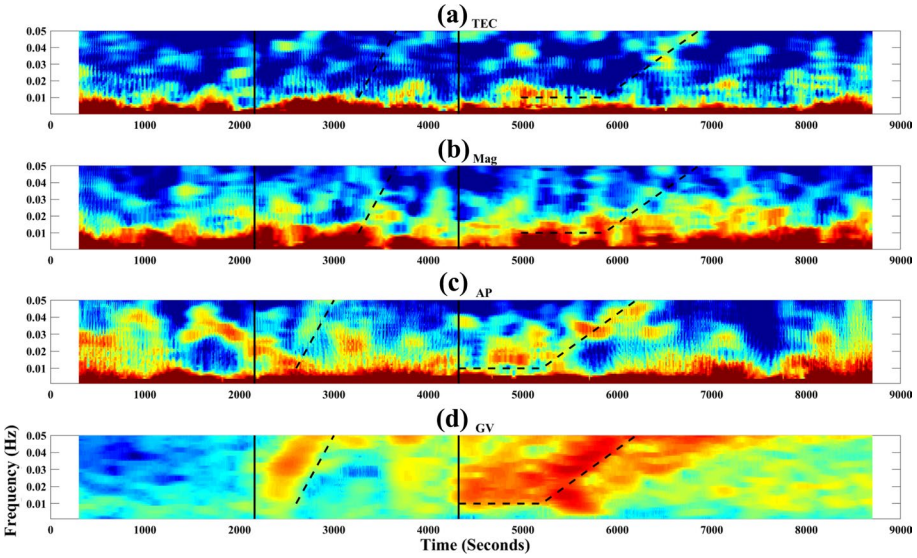

Fig. 4 Amplitude of the total electron content (TEC), magnetic, air pressure, and temperature data from 20:00 to 23:30 (local time) on February 10, 2021; the frequency characteristics of acoustic waves vary from the Earth's surface to the 350 km in altitude. **a**–**d** show the amplitude of the TEC, magnetic (Mag; the magnetic field), air pressure (AP), and seismic (GV; ground vibrations) data using the short-term Fourier transform on February 10, 2021. The vertical black line denotes the arrival time of the surface waves of the studied earthquakes. The dashed lines show the frequency-dependent energy associated with the arrivals of the seismic surface waves. Note that the dashed lines in (**a**) and (**b**) shift 11 min lately for comparison due to temporal period of acoustic wave propagation

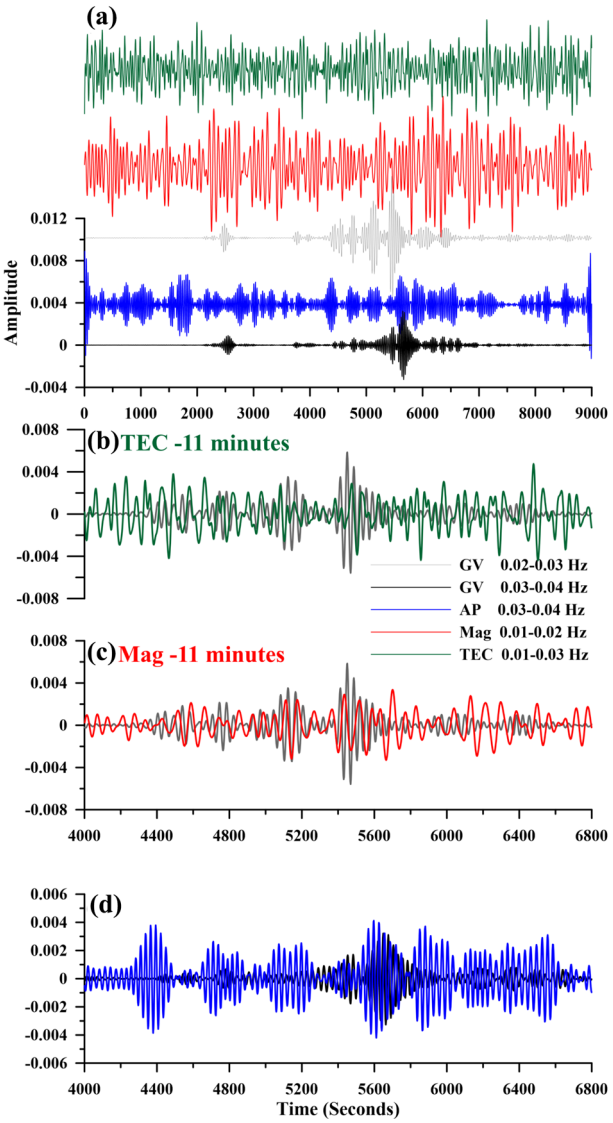

Fig. 5 Filtered data associated with the arrival of seismic waves from 20:00 LT to 23:30 LT on 10 February 2021. Green, red, and blue lines denotes variations of the filtered TEC, Mag, and AP data, respectively. Gray and black lines show the filtered GV data in different frequency bands. **a** shows the filtered data from 20:00 to 23:30; **b–d** reveal the filtered data in a particular segment as the seismic surface waves arrive. Note that the filtered magnetic and TEC data are shifted 11 min early for comparison with the filtered seismic data as the acoustic waves take about 11 min to propagate from the subsurface to the ionosphere at 350 km in altitude in (**b**) and (**c**)

agreement. These results suggest that variations in the TEC are dominated by the upward propagation of acoustic waves excited by the arrival of Rayleigh waves, consistent with the results of previous studies (Liu et al. 2016c; Sun et al. 2016). This suggests that the MVP-LAI system is suitably capable of examining the upward propagation of acoustic waves at different altitudes. In short, the preliminary results of the TEC perturbations excited by the acoustic waves due to the arrival of seismic surface waves and gravity waves (caused by changes in the surface temperature) suggest that the MVP-LAI system exhibits a suitable capability for capturing vibrations and perturbations.

4 Recent Developments and Conclusions

The MVP-LAI system improved the monitoring of electromagnetic signals. Electromagnetic signals play an important role in studying the LAI coupling, such as electromagnetic emission from the ground to the ionosphere, influences of lightning to the ground and the ionosphere, and changes in the conductivity underground, triggering variations in TEC. Currently, the magnetometer in the MVP-LAI system monitors changes in electromagnetic signals, ranging between DC and 10 Hz. This suggests that geomagnetic data records lack observations at relatively high-frequency bands and electric fields near the ground. Therefore, instruments that can simultaneously monitor changes in electromagnetic fields in a relatively high-frequency band will be included in the MVP-LAI system. Note that an atmosphere electric conductivity meter will be installed around the core place to monitor variations in electric conductivity near the Earth's surface. The integration of atmosphere electric conductivity meter provides an excellent opportunity to examine that the role of the electric conductivity in perturbations of the ionosphere from the lithosphere and the atmosphere.

On the other hand, the BDS comprising five geostationary satellites will be further utilized in the MVP-LAI system. A few ground-based GNSS receivers will be established on the north-eastern and north-western sides of the MVP-LAI system, leading to ionospheric pierce points (Liu et al. 1996), which are assumed to be 350 km in altitude, "just" above the MVP-LAI system. The employee of the geostationary satellites produces continuous data in the TEC over the MVP-LAI system without discontinuity due to the GNSS satellite movement. Meanwhile, variations in TEC over the MVP-LAI system can be observed by at least two geostationary satellites that can create an excellent opportunity to double examine the variations using different elevations and azimuth angles.

Additionally, the MVP-LAI system is also located in the high seismicity areas of Sichuan and Yunnan, which is the Sichuan Yunnan Earthquake Science Experimental Park of the China Seismic Experimental Site. High-density geophysical arrays were established in the experimental park for distinct scientific purposes. Once the MVP-LAI system and geophysical arrays are integrated, a three-dimensional monitoring system can be formed. Spatiotemporal variations in the TEC can be monitored using high-density ground-based GNSS stations. Changes in geophysical parameters near the Earth's surface can be understood using multiple arrays. The four-dimensional monitoring system can capture both vertical and oblique vibrations and perturbations with the advantage of fully understanding the causal mechanism of LAI coupling.

Acknowledgements We thank everyone who supported the establishment of the MVP-LAI system and appreciate the interest in the data retrieved from the MVP-LAI system.

Author Contribution C.H.C contributed writing, methodology, formal analysis and revision; Y.Y.S. contributed writing, methodology, discussion and revision; K.L. data collection and discussion; C.Z. contributed data collection and discussion; R.X. contributed data collection and discussion; H.Q. contributed data collection and discussion; Y.G. contributed data collection and discussion; T.C. contributed data collection and discussion; F.W. contributed discussion; H.Y. contributed discussion; P.H. contributed discussion; C.C.T. data collection and discussion; X.S. contributed discussion; X.Z. contributed discussion; L.Y. contributed discussion; Y.X. contributed discussion; J.Y.L. contributed discussion; S.Y. contributed discussion;

Funding This research was funded by the Joint Funds of the National Natural Science Foundation of China (Grant no. U2039205), the National Key Research and Development Project (Grant no. 2018YFE0109700), the Sichuan earthquake Agency-Research Team of GNSS based on geodetic tectonophysics and mantle-crust

dynamics in the Chuan-Dian region (Grant no. 201803), the National Natural Science Foundation of China (Grant no. 41804148, 41804154, 42174211, 11805166, 41774048), the Application Foundation of Science and Technology Department of Sichuan Province (Grant no. 2019YJ0302), the Fundamental Research Funds for the Central Universities, China University of Geosciences (Wuhan) (Grant no. 2018022) and Hefei University of Technology (Grant no. JZ2021HGPB0058). Meanwhile, this work was also supported by the Center for Astronautical Physics and Engineering (CAPE) from the Featured Area Research Center program within the framework of Higher Education Sprout Project by the Ministry of Education (MOE) in Taiwan.

Availability of Data and Materials Daily data have been shown in the website: http://geostation.top. Data are available for directly contacting the first author, Chieh-Hung Chen, through the E-mail: nononochchen@gmail.com.

Declarations

Conflict of interest The authors declare that they have no known competing interests that could have appeared to influence the work reported in this paper.

References

Astafyeva E (2019) Ionospheric detection of natural hazards. Rev Geophys 57:1265–1288. https://doi.org/10.1029/2019RG000668

Bishop RL, Straus PR (2006) Characterizing ionospheric variations in the vicinity of hurricanes and typhoons using GPS occultation measurements, AGU Fall Meeting, San Francisco, 11–15 December, Eos (Trans Am Geophys Union), 87(Suppl.):SA33B-0276

Cander LR (2019) Ionospheric storm morphology. In: Ionospheric space weather. Springer Geophysics, Springer, Cham. Doi:https://doi.org/10.1007/978-3-319-99331-7_5

Chakrabarti SK (eds) (2010) Propagation effects of very low frequency radio waves, conference proceedings 1286, American Institute of Physics

Chang LC, Lin CH, Yue J, Liu JY, Lin JT (2013) Stationary planetary wave and nonmigrating tidal signatures in ionospheric wave 3 and wave 4 variations in 2007–2011 FORMOSAT3/COSMIC observations. J Geophys Res Space Phys 118:6651–6665. https://doi.org/10.1002/jgra.50583

Chang LC, Sun YY, Yue J, Wang JC, Chien SH (2016) Coherent seasonal, annual, and quasi-biennial variations in ionospheric tidal/SPW amplitudes. J Geophys Res Space Phys 121:6970–6985. https://doi.org/10.1002/2015JA022249

Chen CH, Hsu HL, Wen S, Yeh TK, Chang FY, Wang CH, Liu JY, Sun YY, Hattori K, Yen HY (2013) Evaluation of seismo-electric anomalies using magnetic data in Taiwan. Nat Haz Earth Sys 13:597–604

Chen CH, Lin CH, Hsu HL, Wang CH, Lee LC, Han P, Wen S, Chen CS (2015) Evaluating the March 27, 2013 M 6.2 earthquake hypocenter using momentary high-conductivity materials. Terr Atmos Ocean Sci 26:1–9

Chen CH, Lin CH, Yen HY, Chen CR, Jan JC, Wang CH, Liu JY (2017) Artificial magnetic disturbance from the mass rapid transit system in Taiwan. Terra Nova 29:306–311. https://doi.org/10.1111/ter.12277

Chen CH, Lin LC, Yeh TK, Wen S, Yu H, Chen Y, Gao Y, Han P, Sun YY, Liu JY, Lin CH, Tang CC, Lin CM, Hsieh HH, Lu PJ (2020) Determination of epicenters before earthquakes utilizing far seismic and GNSS data: Insights from ground vibrations. Remote Sens 12:3252. https://doi.org/10.3390/rs12193252

Chen CH, Sun YY, Lin LC, Han P, Yu H, Zhang X, Tang CC, Chen CR, Yen HY, Lin CH, Liu JY, Lin CR (2021a) Large air pressure changes triggered by P-SV ground motion in a cave in northern Taiwan. Sci Rep 11:12850. https://doi.org/10.1038/s41598-021-92216-w

Chen CH, Lin JY, Gao Y, Lin CH, Han P, Chen CR, Lin LC, Huang R, Liu JY (2021b) Magnetic pulsations triggered by microseismic ground motion. J Geophys Res 126:e2020JB021416. https://doi.org/10.1029/2020JB021416

Cho M, Rycroft MJ (1998) Computer simulation of the electric field structure and optical emission from cloud-top to the ionospheres. J Atmos Solar-Terr Phys 60:871–888

Chou MY, Lin CCH, Yue J, Tsai HF, Sun YY, Liu JY, Chen CH (2017a) Concentric traveling ionosphere disturbances triggered by Super Typhoon Meranti (2016). Geophys Res Lett 44:1219–1226. https://doi.org/10.1002/2016GL072205

Chou MY, Lin CCH, Yue J, Chang LC, Tsai HF, Chen CH (2017b) Medium-scale traveling ionospheric disturbances triggered by Super Typhoon Nepartak (2016). Geophys Res Lett 44:7569–7577. https://doi.org/10.1002/2017GL073961

Chou MY, Cherniak I, Lin CCH, Pedatella NM (2020) The persistent ionospheric responses over Japan after the impact of the 2011 Tohoku earthquake. Space Weather 18:e2019SW002302. https://doi.org/10.1029/2019SW002302

Chum J, Liu YJ, Laštovička J, Fišer J, Mošna Z, Baše J, Sun YY (2016) Ionospheric signatures of the April 25, 2015 Nepal earthquake and the relative role of compression and advection for Doppler sounding of infrasound in the ionosphere. Earth Planets Space 68:24. https://doi.org/10.1186/s40623-016-0401-9

Davies K (1990) Ionospheric Radio. Peregrinus, London

De la Torre A, Alexander P, Giraldez A (1999) The kinetic to potential energy ratio and spectral separability from high-resolution balloon soundings near the Andes Mountains. Geophys Res Lett 26:1413–1416

Fraser-Smith AC, Bernardi A, McGill PR, Ladd ME, Helliwell RA, Villard OG (1990) Low-frequency magnetic field measurements near the epicenter of the MS7.1 Loma Prieta earthquake. Geophys Res Lett 17(9):1465–1468. https://doi.org/10.1029/GL017i009p01465

Fraser-Smith AC, Kjono SN (2014) The ULF magnetic fields generated by thunderstorms: a source of ULF geomagnetic pulsations? Radio Sci 49(11–12):1162–1170

Gao Y, Harris JM, Wen J, Huang Y, Twardzik C, Chen X, Hu H (2016) Modeling of the coseismic electromagnetic fields observed during the 2004 Mw 6.0 Parkfield earthquake. Geophys Res Lett 43:620–627. https://doi.org/10.1002/2015GL067183

Gao Y, Zhao G, Chong J, Klemperer SL, Han B, Jiang F, Wen J, Chen X, Zhan Y, Tang J, Xiao Q, Wang L (2020) Coseismic electric and magnetic signals observed during 2017 Jiuzhaigou Mw 6.5 earthquake and explained by electrokinetics and magnetometer rotation. Geophys J Int 223(2):1130–1143

Gokhberg MB, Gufeld IL, Rozhnoi AA, Marenko VF, Yampolsky VS, Ponomarev EA (1989) Study of seismic influence on the ionosphere by super long wave probing of the Earth-ionosphere waveguide. Phys Earth Planet Inter 57:64–67

Gufeld IL, Rozhnoi AA, Tyumensev SN, Sherstuk SV, Yampolsky VS (1992) Radiowave disturbances in period to Rudber and Rachinsk earthquakes. Phys Solid Earth 28(3):267–270

Harrison RG, Aplin KL, Rycroft MJ (2010) Atmospheric electricity coupling between earthquake regions and the ionosphere. J Atmos Sol-Terr Phys 72:376–381

Harrison RG, Aplin KL, Rycroft MJ (2014) Brief communication: earthquake–cloud coupling through the global atmospheric electric circuit. Nat Hazards Earth Syst Sci 14:773–777. https://doi.org/10.5194/nhess-14-773-2014

Hayakawa M (2007) VLF/LF radio sounding of ionospheric perturbations associated with earthquakes. Sensors 7:1141–1158

Hayakawa M (2011) Probing the lower ionospheric perturbations associated with earthquakes by means of subionospheric VLF/LF propagation. Earthquake Sci 24(6):609–637

Hayakawa M (2015) Earthquake Prediction with Radio Techniques. John Wiley & Sons, Singapore Pte Ltd, Singapore

Hayakawa M (2016) Earthquake prediction with electromagnetic phenomena. Aip Conference Proceedings

Hayakawa M, Hobara Y (2010) Current status of seismo-electromagnetics for short-term earthquake prediction. Geomatics Nat Hazards Risk 1(2):115–155

Hayakawa M, Kawate R, Molchanov OA, Yumoro K (1996a) Results of ultra-low-frequency magnetic field measurements during the Guam earthquake of 8 August 1993. Geophys Res Left 23:241–244

Hayakawa M, Molchanov OA, Ondoh T, Kawai E (1996b) The precursory signature effect of the Kobe earthquake on VLF subionospheric signals. J Comm Res Lab Tokyo 43:169–180

Hayakawa M, Nakamura T, Hobara Y, Williams E (2004) Observation of sprites over the Sea of Japan and conditions for lightning-induced sprites in winter. J Geophys Res Space Phys 109:A01312. https://doi.org/10.1029/2003JA009905

Hickey MP, Schubert G, Walterscheid RL (2001) Acoustic wave heating of the thermosphere. J Geophys Res Space Phys 106(A10):21543–21548. https://doi.org/10.1029/2001ja000036

Hines CO (1960) Internal atmospheric gravity waves at ionospheric heights. Can J Phys 38(11):1441–1481

Huang YN, Cheng K, Chen SW (1985) On the detection of acoustic-gravity waves generated by typhoon by use of real time HF Doppler frequency shift sounding system. Radio Sci 20:897–906. https://doi.org/10.1029/RS020i004p00897

Inan US, Bell TF, Rodriguez JV (1991) Heating and ionization of the lower ionosphere by lightning. Geophys Res Lett 18:705–708

Immel TJ, Sagawa E, England SL, Henderson SB, Hagan ME, Mende SB, Frey HU, Swenson CM, Paxton LJ (2006) Control of equatorial ionospheric morphology by atmospheric tides. Geophys Res Lett 33:L15108. https://doi.org/10.1029/2006GL026161

Kakinami Y, Kamogawa M, Tanioka Y, Watanabe S, Gusman AR, Liu JY, Watanabe Y, Mogi T (2012) Tsunamigenic ionospheric hole. Geophys Res Lett 39:L00G27. https://doi.org/10.1029/2011GL050159

Kasahara Y, Nakamura T, Hobara Y, Hayakawa M, Rozhnoi A, Solovieva M, Molchanov OA (2010) A statistical study on the AGW modulation in subionospheric VLF/LF propagation data and consideration of the generation mechanism of seismo-ionospheric perturbations. J Atmos Electr 30(2):103–112

Kelley MC, Swartz WE, Heki K (2017) Apparent ionospheric total electron content variations prior to major earthquakes due to electric fields created by tectonic stresses. J Geophys Res Space Phys 122:6689–6695. https://doi.org/10.1002/2016JA023601

Korepanov V, Hayakawa M, Yampolski Y, Lizunov G (2009) AGW as a seismo-ionospheric coupling responsible agent. Phys Chem Earth Parts a/b/c 34(6–7):485–495

Koucká Knížová P, Laštovička J, Kouba D, Mošna Z, Podolská K, Potužníková K, Šindelářová T, Chum J, Rusz J (2021) Ionosphere influenced from lower-Lying atmospheric regions. Front Astron Space Sci 8:651445. https://doi.org/10.3389/fspas.2021.651445

Laštovička J, Šindelářová T (2019) Large-scale and transient disturbances and trends: from the ground to the ionosphere. In: Le-Pichon A, Blanc E, Hauchecorne A (eds) Infrasound monitoring for atmospheric studies. Springer, Cham. https://doi.org/10.1007/978-3-319-75140-5_25

Lin CH, Liu JY, Fang TW, Chang PY, Tasi HF, Chen CH, Hsiao CC (2007) Motions of the equatorial ionization anomaly crests imaged by FORMOSAT-3/ COSMIC. Geophys Res Lett 34:L19101. https://doi.org/10.1029/2007GL030741

Liu JY, Tsai YB, Chen SW, Lee CP, Chen YC, Yen HY, Chang WY, Liu C (2006a) Giant ionospheric disturbances excited by the M9.3 Sumatra earthquake of 26 December 2004. Geophys Res Lett 33:L02103. https://doi.org/10.1029/2005GL023963

Liu JY, Tsai Y, Chen C, Chen Y, Yen H (2016a) Integrated search for Taiwan earthquake precursors (ISTEP). IEEJ Trans Fund Mater 136(5):214–220. https://doi.org/10.1541/ieejfms.136.214

Liu JY, Chang LCW, Chao CK, Chen MQ, Chu YH, Hau LN, Huang CM, Kuo CL, Lee LC, Lyu LH, Lin CH, Pan CJ, Shue JH, Su CL, Tsai LC, Yang YH, Lin CH, Hsu RR, Su HT (2016b) The fast development of solar terrestrial sciences in Taiwan. Geosci Lett 3:1–12. https://doi.org/10.1186/s40562-016-0049-0

Liu JY, Chen CH, Sun YY, Chen CH, Tsai HF, Yen HY, Chum J, Lastovicka J, Yang QS, Chen WS, Wen S (2016c) The vertical propagation of disturbances triggered by seismic waves of the 11 March 2011 M9.0 Tohoku Earthquake over Taiwan. Geophys Res Lett 43:1759–1765. https://doi.org/10.1002/2015GL067487

Liu JY, Sun YY, Kakinami Y, Chen CH, Lin CH, Tsai HF (2011a) Bow and stern waves triggered by the Moon's shadow boat. Geophys Res Lett 38:L17109. https://doi.org/10.1029/2011GL048805

Liu JY, Chen CH, Lin CH, Tsai HF, Chen CH, Kamogawa M (2011b) Ionospheric disturbances triggered by the 11 March 2011 M9.0 Tohoku earthquake. J Geophys Res 116:A06319. https://doi.org/10.1029/2011JA016761

Liu LB, Wan WX (2020) Recent ionospheric investigations in China (2018–2019). Earth Planet Phys 4(3):179–205. https://doi.org/10.26464/epp2020028

Liu YM, Wang JS, Suo YC (2006b) Effects of typhoon on the ionosphere. Adv Geosci 29:351–360

Lucas G, Love JJ, Kelbert A, Bedrosian PA, Rigler EJ (2020) A 100-year geoelectric hazard analysis for the US high-voltage power grid. Space Weather 18:e2019SW002329. https://doi.org/10.1029/2019SW002329

Mao ZQ, Chen CH, Zhang SQ, Yisimayili A, Yu HZ, Yu C, Liu JY (2020) Locating seismo-conductivity anomaly before the 2017 MW 65 Jiuzhaigou earthquake in china using far magnetic stations. Remote Sens 12:1777. https://doi.org/10.3390/rs12111777

Materassi M, Forte B, Coster AJ, Skone S (eds) (2020) The dynamical ionosphere. Elsevier, Amsterdam

Miyaki K, Hayakawa M, Molchanov OA (2002) The role of gravity waves in the lithosphere-ionosphere coupling, as revealed from the subionospheric LF propagation data. In: Hayakawa M, Molchanov OA (eds) Seismo-Electromagnetics (Lithosphere–Atmosphere–Ionosphere Coupling). Terra Scientific Publishing, Tokyo, pp 229–232

Molchanov OA, Hayakawa M (1998) Subionospheric VLF signal perturbations possibly related to earthquakes. J Geophys Res 103:17489–17504

Molchanov OA, Hayakawa M, Miyaki K (2001) VLF/LF sounding of the lower ionosphere to study the role of atmospheric oscillations in the lithosphere-ionosphere coupling. Adv Polar Upper Atmos Res Tokyo 15:146–158

Molchanov OA, Mazhaeva OA, Goliavin AN, Hayakawa M (1993) Observations by the intercosmos-24 satellite of ELF-VLF electromagnetic emissions associated with earthquakes. Ann Geophys 11:431–440

Molchanov OA, Hayakawa M (1995) Generation of ULF electromagnetic emissions by microfracturing. Geophys Res Lett 22:3091–3094

Molchanov OA, Hayakawa M, Rafalsky VA (1995) Penetration characteristics of electromagnetic emissions from an underground seismic source into the atmosphere, ionosphere and magnetosphere. J Geophys Res 100:1691–1712

Nishioka N, Tsugawa T, Kubota M, Ishii M (2013) Concentric waves and short-period oscillations observed in the ionosphere after the 2013 Moore EF5 tornado. Geophys Res Lett 40:5581–5586

Oyama KI, Kakinami Y, Liu JY, Kamogawa M, Kodama T (2008) Reduction of electron temperature in low-latitude ionosphere at 600 km before and after large earthquakes. J Geophys Res 113:A11317. https://doi.org/10.1029/2008JA013367

Oyama KI, Devi M, Ryu K, Chen CH, Liu JY, Liu H, Bankov L, Kodama T (2016) Modifications of the ionosphere prior to large earthquakes: report from the ionospheric precursor study group. Geosci Let 3(1):6. https://doi.org/10.1186/s40562-016-0038-3

Parkinson WD (1962) The influence of continents and oceans on geomagnetic variations. Geophys J R Astron Soc 6:441–449. https://doi.org/10.1111/j.1365-246X.1962.tb02992.x

Parkinson WD, Jones FW (1979) The geomagnetic coast effect. Rev Geophys 17:1999–2015

Pasko VP, Inan US, Bell TF, Taranenko YN (1997) Sprites produced by quasi-electrostatic heating and ionization in the lower ionosphere. J Geophys Res Space Phys 102(A3):4529–4561. https://doi.org/10.1029/96JA03528

Polyakova AS, Perevalova NP (2011) Investigation into impact of tropical cyclones on the ionosphere using GPS sounding and NCEP/NCAR Reanalysis data. Adv Space Res 48:1196–1210

Pulinets SA (2009) Physical mechanism of the vertical electric field generation over active tectonic faults. Adv Space Res 44(6):767–773

Pulinets SA, Boyarchuk K (2004) Ionospheric precursors of earthquakes. Springer, Berlin

Pulinets SA, Ouzounov D (2011) Lithosphere– atmosphere–ionosphere coupling (LAIC) model—a unified concept for earthquake precursors validation. J Asian Earth Sci 41:371–382

Rajesh PK, Lin CH, Lin CY, Chen CH, Liu JY, Matsuo T, Chen SP, Yeh WH, Huang CY (2021) Extreme positive ionosphere storm triggered by a minor magnetic storm in deep solar minimum revealed by formosat-7/cosmic-2 and GNSS observations. J Geophys Res Space Phys 126:e2020JA028261. https://doi.org/10.1029/2020JA028261

Rishbeth H (2006) F-region links with the lower atmosphere? J Atmos Solar-Terr Phys 68:469–478

Rodger CJ (1999) Red sprites, upward lighting and VLF perturbations. Rev Geophys 37:317–336

Rozhnoi A, Solovieva M, Hayakawa M (2013) VLF/LF signals method for searching of electromagnetic earthquake precursors. In: Hayakawa M (ed) Earthquake prediction studies: seismo electromagnetics. Terra Scientific Publishing, Tokyo, pp 31–48

Ryu K, Parrot M, Kim SG, Jeong KS, Chae JS, Pulinets S, Oyama KI (2015) Suspected seismo-ionospheric coupling observed by satellite measurements and GPS TEC related to the M7.9 Wenchuan earthquake of 12 May 2008. J Geophys Res Space Phys 119:10305–10323. https://doi.org/10.1002/2014JA020613

Shen X, Zhang H, Yuan X, Wang SG, Cao LW, Huang JB, Zhu JP, Piergiorgio XH, Dai JP (2018a) The state-of-the-art of the China seismo-electromagnetic satellite mission. Sci China Technol Sci 61:634–642

Shen XH, Zong QG, Zhang X (2018b) Introduction to special section on the China seismo-electromagnetic satellite and initial results. Earth Planet Phys 2:439–443

Shvets AV, Hayakawa M, Molchanov OA, Ando Y (2004) A study of ionospheric response to regional seismic activity by VLF radio sounding. Phys Chem Earth 29:627–637

Sorokin V, Chemyrev V, Hayakawa M (2015) Electrodynamic coupling of lithosphere-atmosphere-ionosphere of the earth. Nova Science Publishing

Sorokin VM, Yaschenko AK, Chmyrev VM, Hayakawa M (2006) DC electric field amplification in the mid-latitude ionosphere over seismically active faults. Phys Chem Earth 31:447–453

Su X, Meng G, Sun H, Wu W (2018) Positioning performance of BDS observation of the crustal movement observation network of China and its potential application on crustal deformation. Sensors 18:3353. https://doi.org/10.3390/s18103353

Sun YY (2019) GNSS brings us back on the ground from ionosphere. Geosci Lett 6:14. https://doi.org/10.1186/s40562-019-0144-0

Sun YY, Lin JY, Lin CY, Tasi HF, Chang LC, Chen CY, Chen CH (2016) Ionospheric F2 region perturbed by the 25 April 2015 Nepal earthquake. J Geophys Res Space Phys 121:5778–5784. https://doi.org/10.1002/2015JA022280

Sun YY, Liu H, Miyoshi Y, Chang LC, Liu L (2019) El Niño – Southern Oscillation effect on ionospheric tidal/SPW amplitude in 2007–2015 FORMOSAT-3/COSMIC observations. Earth Plant Space 71:35. https://doi.org/10.1186/s40623-019-1009-7

Sun YY, Liu HX, Miyoshi Y, Liu LB, Chang LC (2018) El Niño-Southern Oscillation effect on quasi-biennial oscillations of temperature diurnal tides in the mesosphere and lower thermosphere. Earth Planets Space 70:85. https://doi.org/10.1186/s40623-018-0832-6

Sun YY, Oyama KI, Liu JY, Jhuang HK, Cheng CZ (2011) The neutral temperature in the ionospheric dynamo region and the ionospheric F region density during Wenchuan and Pingtung Doublet earthquakes. Nat Hazard Earth Sys 11:1759–1768. https://doi.org/10.5194/nhess-11-1759-2011

Sun YY, Chen CH, Qing H, Xu R, Su X, Jiang C, Yu T, Wang J, Xu H, Kai L (2021a) Nighttime ionosphere perturbed by the annular solar eclipse on 21 June 2020. J Geophys Res Space Phys 126:e2021JA029419. https://doi.org/10.1029/2021JA029419

Sun YY, Shen MM, Tsai YL, Lin CY, Chou MY, Yu T, Kai L, Huang Q, Wang J, Qiu L, Chen CH, Liu JY (2021b) Wave steepening in ionospheric total electron density due to the 21 August 2017 total solar eclipse. J Geophys Res Space Phys 126:e2020JA028931. https://doi.org/10.1029/2020JA028931

Takahashi Y, Miyasato R, Adachi T, Adachi K, Sera M, Uchida A, Fukunishi H (2003) Activities of sprites and elves in the winter season, japan. J Atmos Solar-Terr Phys 65(5):551–560

Tsuda T, Murayama Y, Nakamura T, Vincent RA, Manson AH, Meek CE, Wilson RL (1994) Variations of the gravity wave characteristics with height, season and latitude revealed by comparative observations. J Atmos Sol Terr Phys 56:555–568

VanZandt TE (1985) A model for gravity wave spectra observed by Doppler sounding systems. Radio Sci 20:1323–1330

Wan W, Liu L, Pi X, Zhang ML, Ning B, Xiong J, Ding F (2008) Wavenumber-4 patterns of the total electron content over the low latitude ionosphere. Geophys Res Lett 35:L12104. https://doi.org/10.1029/2008GL033755

Wang J, Zuo X, Sun YY, Yu T, Wang Y, Qiu L, Mao T, Yan X, Yang N, Qi Y, Lei J, Sun L, Zhao B (2021) Multilayered sporadic-E response to the annular solar eclipse on June 21, 2020. Space Weather 19:e2020SW002643. https://doi.org/10.1029/2020SW002643

Xiao Z, Xiao SG, Hao YQ, Zhang DH (2007) Morphological features of ionospheric response to typhoon. J Geophys Res Space Phys 112:A04304. https://doi.org/10.1029/2006JA011671

Xu G, Wan W, She C, Du L (2008) The relationship between ionospheric total electron content (TEC) over East Asia and the tropospheric circulation around the Qinghai-Tibet Plateau obtained with a partial correlation method. Adv Space Res 42:219–223

Yamazaki Y, Maute A (2016) Sq and EEJ—a review on the daily variation of the geomagnetic field caused by ionospheric dynamo currents. Space Sci Rev 206:299–405

Yan X, Sun YY, Yu T, Liu JY, Qi Y, Xia C, Zuo X, Yang N (2018) Stratosphere perturbed by the 2011 Mw9.0 Tohoku earthquake. Geophys Res Lett 45:10050–10056. https://doi.org/10.1029/2018GL079046

Yang SS, Hayakawa M (2020) Gravity wave activity in the stratosphere before the 2011 Tohoku earthquake as the mechanism of lithosphere-atmosphere-ionosphere coupling. Entropy 22:110

Yang SS, Potirakis SM, Sasmal S, Hayakawa M (2020) Natural time analysis of global navigation satellite system surface deformation: the case of the 2016 Kumamoto earthquakes. Entropy 22(6):674

Zhou C, Liu Y, Zhao S, Liu J, Zhang X, Huang J, Shen X, Ni B, Zhao Z (2017) An electric field penetration model for seismo-ionospheric research. Adv Space Res 60(10):2217–2232. https://doi.org/10.1016/j.asr.2017.08.007

Authors and Affiliations

Chieh-Hung Chen[1,2] · Yang-Yi Sun[1] · Kai Lin[1] · Chen Zhou[3] · Rui Xu[4] · Haiyin Qing[5] · Yongxin Gao[6] · Tao Chen[7] · Fei Wang[8] · Huaizhong Yu[9] · Peng Han[10] · Chi-Chia Tang[1] · Xiaoning Su[11] · Xuemin Zhang[12] · Linguo Yuan[13] · Yixian Xu[14] · Jann-Yenq Liu[15,16,17] · Shunkuan Yu[18]

1 Institute of Geophysics and Geomatics, China University of Geosciences, Wuhan 430074, Hubei, China

2 State Key Laboratory of Geological Processes and Mineral Resources, China University of Geosciences, Wuhan 430074, China

3 Department of Space Physics, School of Electronic Information, Wuhan University, Wuhan 430072, China

4 Sichuan Earthquake Bureau, Chengdu 610041, China

5 School of Electronics and Materials Engineering, Leshan Normal University, Sichuan 614000, China

6 School of Civil Engineering, Hefei University of Technology, Hefei 230009, China

7 National Space Science Center, Chinese Academy of Sciences, Beijing 100049, China

8 Chengdu University of Technology, Chengdu 610059, China

9 China Earthquake Networks Center, Beijing 100045, China

10 Department of Earth and Space Sciences, Southern University of Science and Technology, Shenzhen 518055, China

11 Faculty of Geomatics, Lanzhou Jiaotong University, Lanzhou 730070, China

12 Institute of Earthquake Forecasting, China Earthquake Administration, Beijing 100036, China

13 Faculty of Geosciences and Environmental Engineering, Southwest Jiaotong University, Chengdu 611756, China

14 School of Earth Sciences, Zhejiang University, Hangzhou 310027, Zhejiang, China

15 Department of Space Science and Engineering, National Central University, Taoyuan 320317, Taiwan

16 Center for Space and Remote Sensing Research, National Central University, Taoyuan 320317, Taiwan

17 Center for Astronautical Physics and Engineering, National Central University, Taoyuan 320317, Taiwan

18 Wuhan Goldwell Information Technology Co. Ltd, Wuhan 430070, China